Modeling Membrane Deformations and Lipid Demixing upon Protein-Membrane Interaction: The BAR Dimer Adsorption

George Khelashvili,[†*] Daniel Harries,[‡*] and Harel Weinstein[†§]
[†]Department of Physiology and Biophysics, Weill Medical College of Cornell University, New York, New York; [‡]Institute of Chemistry and the Fritz Haber Research Center, The Hebrew University, Jerusalem, Israel; and [§]The HRH Prince Alwaleed Bin Talal Bin Abdulaziz Alsaud Institute for Computational Biomedicine, New York, New York

ABSTRACT We use a self-consistent mean-field theory, designed to investigate membrane reshaping and lipid demixing upon interaction with proteins, to explore BAR domains interacting with large patches of lipid membranes of heterogeneous compositions. The computational model includes contributions to the system free energy from electrostatic interactions and elastic energies of the membrane, as well as salt and lipid mixing entropies. The results from our simulation of a single adsorbing Amphiphysin BAR dimer indicate that it is capable of stabilizing a significantly curved membrane. However, we predict that such deformations will occur only for membrane patches that have the inherent propensity for high curvature, reflected in the tendency to create local distortions that closely match the curvature of the BAR dimer itself. Such favorable preconditioning for BAR-membrane interaction may be the result of perturbations such as local lipid demixing induced by the interaction, or of a prior insertion of the BAR domain's amphiphatic N-helix. From our simulations it appears that local segregation of charged lipids under the influence of the BAR dimer cannot produce high enough asymmetry between bilayer leaflets to induce significant bending. In the absence of additional energy contributions that favor membrane asymmetry, the membrane will remain nearly flat upon single BAR dimer adsorption, relative to the undulation expected from thermal fluctuations. Thus, we conclude that the N-helix insertions have a critical mechanistic role in the local perturbation and curving of the membrane, which is then stabilized by the electrostatic interaction with the BAR dimer. We discuss how these results can be used to estimate the tendency of BARs to bend membranes in terms of a spatially nonisotropic spontaneous curvature.

INTRODUCTION

The recognition of local architectural features of cell membranes, as well as local reshaping of membranes, are gaining attention as mechanistic steps in cell signaling and physiological function (1–3). We have previously presented a self-consistent mean-field model that allows for calculation of the equilibrium configuration and binding energies of protein-membrane interactions. Here we show that this method can successfully describe the BAR-domain induced remodeling of a heterogeneous membrane. BAR domains are of great interest in cell physiological processes (4–6). They are known to dimerize into a bananalike molecular structure (7) that faces a lipid membrane with its concave surface (Fig. 1, *A* and *B*). The interactions of BAR domain dimers (referred to as BAR, for simplicity) with the cell membrane are associated with a curving of the interface regions that often contain a relatively higher concentration of negatively charged lipids (3,8–10). The functional role of such membrane remodeling by BARs appears to be a clustering localized in specialized membrane regions and is likely to be important for signaling (11). Some BAR domains (termed N-BARs) have N-terminal regions that appear to fold into amphipathic helices upon BAR-membrane binding, and to insert into the polar headgroup region of lipid membranes (10,12–21).

In the transformation of a membrane that is spontaneously flat at equilibrium into a highly curved structure, BAR appears to take advantage of a special set of structural features (see Elements of Membrane Remodeling in the Supporting Material). Experimental evidence suggests that global membrane remodeling events triggered by BAR domains, such as vesiculation and tubulation, are driven by multiple BARs that jointly assemble at membrane surfaces. Thus, recent theoretical work by Arkhipov et al. (22) predicted that BAR modules achieve membrane reshaping when they are in a two-row staggered arrangement, but fail to do so when they are aligned in one line. Ayton et al. (23) used mesoscopic simulations and showed that liposome tubulation can result from anisotropic N-BAR spontaneous curvature fields, whereas spherical vesiculation is only observed with isotropic N-BAR spontaneous curvature fields at high density.

Still, because proteins containing single BAR domain can participate in cell signaling (11), to understand their role in the signal transduction process it is essential to address the membrane remodeling process at the level of a single BAR. To this end, Blood and co-workers (24,25) performed molecular dynamics (MD) simulations of Amphiphysin N-BAR domain interacting with lipid membrane. Their calculations revealed how a single N-BAR induces strong local membrane curvature (24), and further studies showed (25) that Amphiphysin N-BAR domain lacking key positive residues on its concave surface failed to drive significant local membrane deformations even when their N-terminal

Submitted March 16, 2009, and accepted for publication July 7, 2009.

*Correspondence: gek2009@med.cornell.edu or daniel@fh.huji.ac.il

Editor: Peter Tieleman.

0006-3495/09/09/1626/10 $2.00

doi: 10.1016/j.bpj.2009.07.006

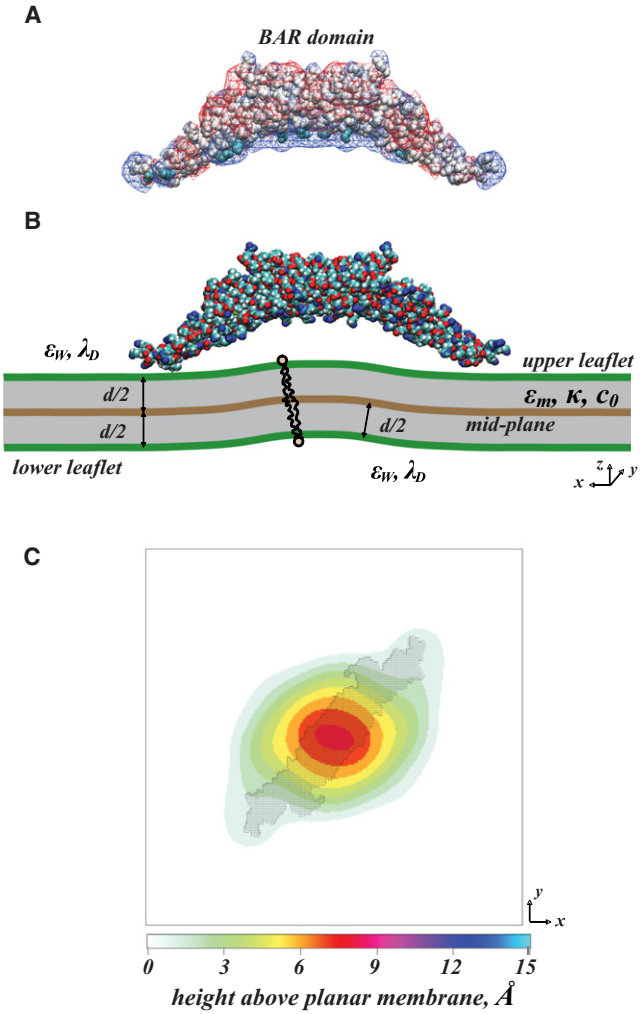

FIGURE 1 Color online only. (*A*) Amphiphysin BAR domain (Protein Data Bank ID code 1URU). Three-dimensional structure of the BAR domain dimer is shown in space-fill representation, with positively charged residues on the concave surface highlighted in light blue. Electrostatic potential isosurfaces, as calculated from the nonlinear PB theory using the APBS software, are shown in red (−25 mV equipotential contour) and blue (+25 mV equipotential contour) meshes, respectively. (*B*) Side view of the BAR-membrane system at steady state, as predicted from our model calculations (adopted from Fig. 3 and discussed in the Results). For this calculation, the membrane with a homogeneous surface charge density of $\sigma = -0.004e/\text{Å}^2$ on both leaflets (corresponding to $\phi^0_{PS} = 0.3$) was characterized by a bending modulus of $\kappa_m = 10\ k_BT$ and a spontaneous curvature $c_0 = 1/70\ \text{Å}^{-1}$ near the adsorbed protein. BAR is shown in space-fill; the membrane interior is shaded gray. Charges on the lipid headgroups are represented by continuous surface charge densities on the two leaflets (drawn as *green curves*), and the bilayer midplane is colored in brown. Membrane thickness $d = 40$ Å is constant across the membrane. In all our calculations the dielectric constant is $\varepsilon_m = 2$ for the membrane interior as well as protein; the dielectric constant of the aqueous environment is $\varepsilon_m = 80$, and the Debye length of the electrolyte solution is $\lambda_D = 10$ Å. (*C*) Height profile of the membrane upper leaflet from calculations described in panel *B*. Color code shows contours of local heights attained by the upper leaflet, with white (zero height) representing a flat membrane. For completeness, we also illustrate the orientation of the BAR domain used in all our calculations with respect to *x* and *y* axis of the membrane plane, by plotting in dark shades the projection of the BAR domain onto a (*x*,*y*) plane. The BAR orientation is omitted from subsequent figures for clarity.

helices embedded into the bilayer. On the other hand, N-BAR that did not have its N-helices inserted into the membrane was incapable of inducing any curvature. In addition, N-BAR domains showed stable binding to PIP_2-containing membrane even without their helices embedded in the bilayer. Using a more coarse-grained representation for the lipid membrane, Campelo et al. (26) predicted that N-helical insertions alone are sufficient to drive significant membrane curvatures.

In view of the critical role of both electrostatic interactions and amphipathic helix insertions in the process of membrane remodeling by BAR domains, some fundamental questions have remained unanswered. These include the equilibrium state of a single BAR-membrane assembly and binding energies of BAR-membrane complexes, as well as the nature of the coupling between electrostatically driven lipid sequestration and local membrane curvature. Addressing these issues enables answers to specific questions such as whether the BAR-induced segregation of polyvalent PIP_2 lipids can be the source of substantial membrane deformation, and how the N-helix insertions might complement this coupling.

To address such questions, we employ a model that extends our self-consistent mean-field theory described recently (27) to calculations of equilibrium lipid distribution and membrane shape under an adsorbing BAR, as well as provides steady-state binding energies of the BAR-membrane assembly. Furthermore, our model investigates whether BAR-induced sequestration of PIP_2 lipids can lead to substantial membrane deformation, and studies the role of N-helix insertions.

THE MODEL

The mean-field level model for a single BAR-membrane system closely follows the formalism outlined in Khelashvili et al. (27) and Harries et al. (28), where additional details can be found. Within our approach, the free energy density functional governing the system is based on the continuum Helfrich free energy for membrane elasticity (29), and on the nonlinear Poisson-Boltzmann (PB) theory of electrostatics (30–36). Providing realistic three-dimensional treatment of the electrostatic problem and requiring only a few phenomenological material constants to describe the lipid bilayer, this simple formalism accounts for a number of important membrane properties. Although this mesoscopic theory neglects most atomic structural features of a lipid bilayer (37,38), similar membrane and membrane-macromolecule models have been shown to yield reliable qualitative and quantitative predictions (27,28,37–47).

We focus on a unit simulation cell that contains a single Amphiphysin BAR domain in atomistic three-dimensional detail adsorbed on a lipid membrane immersed in an aqueous solution of dielectric $\varepsilon = 80$, and surrounded by its periodic replicas(see Fig. 1 *A*). The solution also contains a symmetric 1:1 electrolyte of bulk concentration n_0. We consider the limit of low surface density of adsorbing proteins, so that the

interaction between BARs is negligible. Both BAR and lipid bilayer are treated as a low dielectric material, with dielectric constant $\varepsilon_m = 2$ within protein and membrane. The BAR is fixed in space near the membrane in an orientation with its long axis parallel to the flat membrane's (x,y) plane, and the short axis perpendicular to that plane (along z) as depicted in Fig. 1 *B* (see the Supporting Material).

The membrane is represented as a two-dimensional incompressible, tensionless, elastic medium (48) comprised of two-dimensional smooth charged surfaces where the lipid polar headgroups reside, and a low-dielectric hydrophobic core volume (Fig. 1 *B*). Using the continuum representation, the hydrophilic boundaries are considered to be composed of mixtures of m_u and m_l lipids, where the subscripts u and l refer to upper and lower leaflets, respectively (Fig. 1 *B*). For simplicity, we discuss here membranes composed of binary mixtures of charged and neutral lipids (though the treatment can be easily generalized to any number of lipid species, in the spirit of Khelashvili et al. (27)), with the local mole fractions of charged lipid species on the two layers represented by ϕ_u and ϕ_l. Assuming the same lateral area per headgroup for both lipids, a, we define the local surface charge densities on the two planes,

$$\begin{aligned}\sigma_u &= \frac{e}{a}\phi_u\zeta_u \\ \sigma_l &= \frac{e}{a}\phi_l\zeta_l\end{aligned} \tag{1}$$

where ζ_u and ζ_l denote the valencies of charged lipids on the upper and lower leaflets, respectively.

The distance d between the two charged monolayer interfaces is the minimum distance between them; assuming the thickness of the membrane to be constant throughout the bilayer, d has a single value everywhere (Fig. 1 *B*) (37,39,40). We focus on bilayer bending as the most relevant deformation mode, and in this study, neglect any dilation-induced or lipid tilt-related membrane deformations (37,39,40). Membrane geometry is described by the contours of these interfacial surfaces, with the simplifying assumption that the locations of the two charged interfaces coincide with the positions of the neutral planes of the respective membrane layers (49).

The free energy functional describing the system is a sum of electrostatic energy, mobile salt ion translational entropy, lipid mixing entropy, membrane bending energy, and the repulsive short-range interaction energy between protein and membrane interfaces (27,28,43,44):

$$F = F_{el} + F_{IM} + F_{lip} + F_b + F_{rep}. \tag{2}$$

The system's electrostatic (Coulomb) energy is given as usual by

$$F_{el} = \frac{1}{2}\varepsilon_0\varepsilon_w\left(\frac{k_BT}{e^2}\right)\int_V (\nabla\Psi)^2 dv. \tag{3}$$

Here $\Psi = e\Phi/k_BT$ is the dimensionless (reduced) electrostatic potential, with Φ as the electrostatic potential, k_B the Boltzmann's constant, T the temperature, and e the elementary charge; ε_0 is the permeability of free space; and $\varepsilon_w = 80$ is the dielectric constant of the aqueous solution.

The contribution from the translational entropy of mobile (salt) ions in solution is

$$F_{IM} = k_BT\int_V \left[n_+\ln\frac{n_+}{n_0} + n_-\ln\frac{n_-}{n_0} - (n_+ + n_- - 2n_0)\right]dv, \tag{4}$$

where n_+ and n_- are local concentrations of (+) and (−) mobile electrolyte ions, respectively, and n_0 is the electrolyte concentration in the bulk.

The contribution from the two-dimensional mixing entropy due to mobile lipid molecules within each leaflet is

$$\begin{aligned}F_{lip} = {} & \frac{k_BT}{a}\int_{A_u} dA_u\left[\phi_u\ln\frac{\phi_u}{\phi_u^0} + (1-\phi_u)\ln\frac{(1-\phi_u)}{(1-\phi_u^0)}\right] \\ & + \frac{k_BT}{a}\int_{A_l} dA_l\left[\phi_l\ln\frac{\phi_l}{\phi_l^0} + (1-\phi_l)\ln\frac{(1-\phi_l)}{(1-\phi_l^0)}\right].\end{aligned} \tag{5}$$

Both integrals represent entropic penalties associated with lipid demixing (27,43), on the upper and the lower surfaces of the membrane, respectively, due to lipid segregation, and ϕ_u^0 and ϕ_l^0 denote the average compositions of charged lipids on the respective leaflets.

The membrane bending energy in Eq. 2 is the sum of elastic energies associated with deformations of individual membrane leaflets away from their spontaneous curvatures and is given by the Helfrich expression (29)

$$F_b = \frac{1}{2}\kappa_m\int_{A_u} dA_u\left(c_u - c_u^0(\phi_u)\right)^2 + \frac{1}{2}\kappa_m\int_{A_l} dA_l\left(c_l - c_l^0(\phi_l)\right)^2, \tag{6}$$

where the integrations are over the membrane upper and lower leaflets. In Eq. 6, c_u and c_l are the local mean curvatures of the bilayer upper and lower planes. Following the standard convention, we assign positive curvature bending toward the solvent, and negative for bending away from it. Bending rigidities κ_m in Eq. 6 are the same for each monolayer, and we assume κ_m to be equal for all lipids, and therefore independent of local lipid fractions. The spontaneous curvatures of the two leaflets, c_u^0 and c_l^0, originating from the molecular shapes and interactions, are generally more sensitive to the local lipid composition (37,50). Following the work in Harries et al. (28) and Andelman et al. (51), we define the locally varying c^0-values as weighted sums of the spontaneous curvatures of the pure lipid constituents,

$$\begin{aligned}c_u^0 &= c_c^0\phi_u + c_n^0(1-\phi_u) \\ c_l^0 &= c_c^0\phi_l + c_n^0(1-\phi_l),\end{aligned} \tag{7}$$

where c_c^0 and c_n^0 denote the spontaneous curvatures of the pure charged and neutral lipids, respectively.

Note that BAR binding to the membrane breaks the in-plane rotational symmetry inherent to the bare homogeneous lipid membranes (see Discussion). This is due to the strongly anisotropic electrostatic interactions between BAR and the membrane, which results in anisotropic membrane deformations (24,25). Clearly, this should be reflected in the results from the full self-consistent free energy minimization scheme, because the bending free energy term in Eq. 6 alone, without the other energy contributions in Eq. 2, cannot describe anisotropic curvature, as the Helfrich model is rotationally invariant (52). To achieve the anisotropic deformation of the membrane, Ayton et al. (23) enhanced their elastic model with a deviatoric energy term that was required because the electrostatic interactions were not considered explicitly in that model. In contrast, here the electrostatic contributions are considered explicitly and in a self-consistent manner together with the elastic energy contributions (see below and in the Supporting Material). Thus, the anisotropic nature of the BAR-induced perturbations should be reflected in our model as anisotropic curvatures around the adsorbed BAR without any a priori assumption about BAR-induced spontaneous curvature fields and without the need for additional energy contributions, such as deviatoric energy terms.

Finally, the repulsive free energy term in Eq. 2, F_{rep}, arises when two surfaces (protein and membrane) come close to each other, and accounts for short-ranged interactions, such as excluded volume and hydration contributions (53–56). We treat F_{rep} as a hard wall potential that restricts the membrane-protein minimal approach to be ≥ 2 Å, and therefore exclude any configuration that violates this limitation.

Minimization of the free energy functional with respect to mobile ion concentrations is carried out within the nonlinear PB theory (27,30–36,44); the Cahn-Hilliard formalism is used as discussed in detail in Khelashvili et al. (27) to relax the lipid compositional degrees of freedom (57). Optimization of the membrane shape is performed self-consistently together with the electrostatic and repulsive interactions, as well as lipid mixing. This combined scheme, which self-consistently converges to the (local) minimum of the total free energy, is detailed in the Supporting Material.

RESULTS

From application to amphiphysin bar domain adsorption on mixed membranes

Lipid demixing alone is insufficient to induce significant membrane curvatures

Fig. 2 shows calculated lipid segregation and bilayer deformations for the equilibrium state of the Amphyphysin BAR adsorbing on compositionally symmetric binary mixtures of PS/PC (*lower panels*) and PIP_2/PC (*upper panels*). The membrane patches contain $\phi^0_{PS} = 0.3$ or $\phi^0_{PIP_2} = 0.04$, and are characterized by a bending modulus per monolayer of $\kappa_m = 10\ k_BT$, a value common to many lipid membranes (58). The BAR domain positioned near the bilayers remains fixed in space with the orientation depicted in Fig. 1, *B* and *C*. Fig. 1, *A–D*, shows equilibrium membrane deformation contours for PIP_2/PC and PS/PC membranes in terms of local heights on the upper and lower leaflets. Fig. 2, *E–H*, detail the extent of lipid segregation on the upper and lower monolayers at equilibrium reported as relative values (local to average lipid fraction) $\phi^*_\alpha(\vec{r}) = \phi_\alpha(\vec{r})/\phi^0_\alpha$ (α = PS, PIP_2).

The results of the free energy minimization procedure (described in the Supporting Material) reveal weak membrane deformations at equilibrium under the influence of the adsorbing BAR for both PS- and PIP_2-containing membranes (Fig. 2, *A–D*). In fact, for both PS and PIP_2 mixtures, the largest membrane deformations found in the center of the patches, reach only ~3–4 Å above the height of the planar membrane. This value is comparable to the expected thermal undulations of the membrane at a temperature T and bending rigidity κ. For a periodic membrane of lateral area A undulating freely, the amplitude h_{und} was shown to be (59)

$$\langle h^2_{und} \rangle \approx \frac{k_B T A}{8.3\pi^3 \kappa}, \tag{8}$$

corresponding to h_{und} ~4 Å for our patches. Therefore, the BAR-related deformations do not extend beyond the expected membrane fluctuations.

These insignificant membrane curvatures are accompanied by only minor segregation of charged lipid around the adsorbing protein in both bilayer mixtures (Fig. 2, *E–H*). Because both PS and PIP_2 have positive spontaneous curvatures, their strong aggregation on one leaflet near the BAR domain might be expected to create local asymmetry in the membrane. This would favor a bent bilayer at steady state, which in turn, would act synergistically with the pure Coulombic interactions to form membranes with positive curvature. But Fig. 2 *E* reveals that on the BAR-facing leaflet of the PIP_2-containing membrane, the PIP_2 lipid levels are elevated by only ~1.3 times their 4% bulk value, even in the regions of strongest aggregation (*dark blue shades*). These PIP_2-enriched patches appear near the positively charged tips of the BAR domain, and their formation is the result of strong electrostatic interactions with negatively charged PIP_2 lipid headgroups (see also Fig. 1 *A*). Somewhat weaker sequestration of PIP_2 is also observed close to the center of the upper leaflet (*lighter blue shades* in Fig. 2 *C*). As expected, localization of PIP_2 in these areas is due not only to electrostatic forces between the BAR and the membrane, but also to elastic forces within the bilayer that favor relocation of PIP_2 lipids to the regions of positive curvature.

Fig. 2 *G* shows that PS lipid distribution on the BAR-facing leaflet of the PS-containing membrane follows a similar pattern to that observed for PIP_2 lipids, but the sequestration of PS lipids is even less pronounced. The finding that peripheral proteins can generally segregate polyvalent lipids to

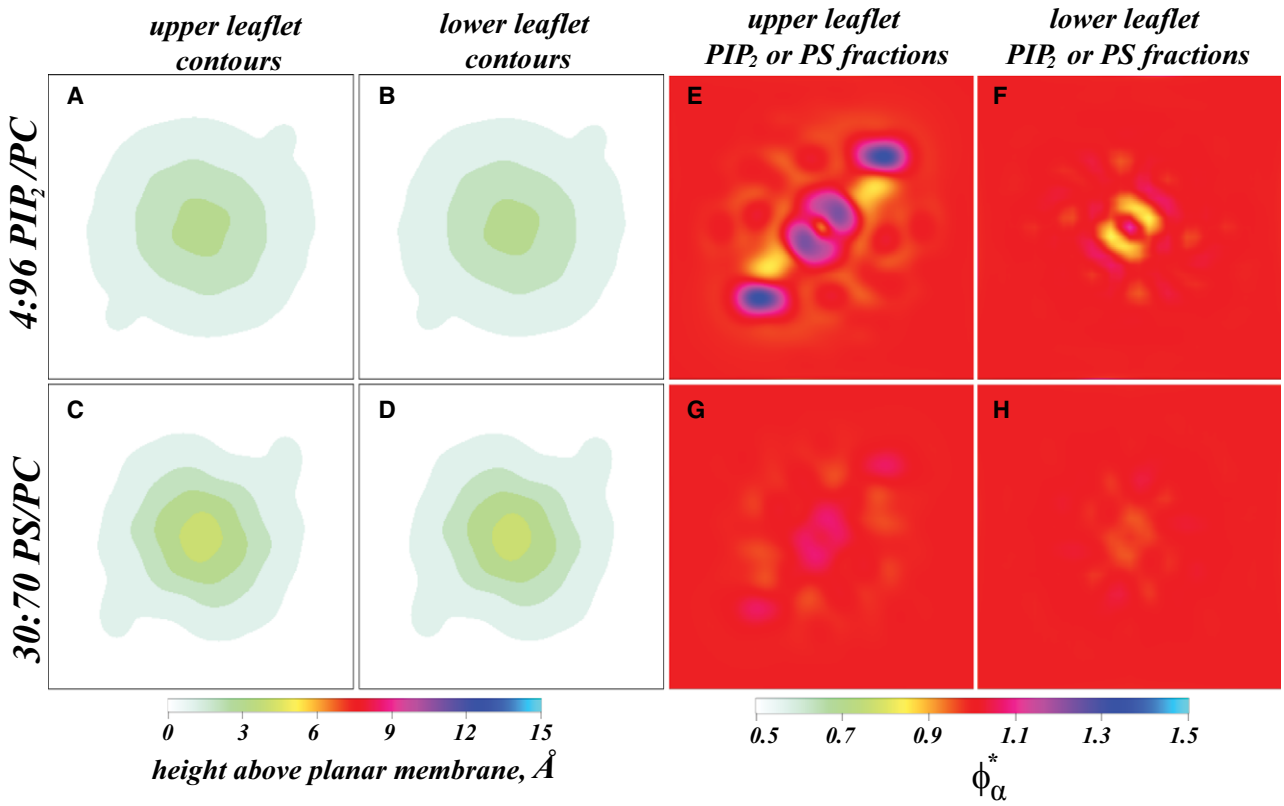

FIGURE 2 Color online only. Adsorption of the Amphiphysin BAR domain on compositionally symmetric binary mixtures of PS/PC (*lower panels*) and PIP_2/PC (*upper panels*). The membrane patches are characterized by bending modulus of $\kappa = 20\ k_BT$, and contain $\phi^0_{PS} = 0.3$ and $\phi^0_{PIP_2} = 0.04$, respectively. The lipids are described by spontaneous curvatures of $c_{PS}{}^0 = 1/144\ Å^{-1}$, $c_{PC}{}^0 = -1/100\ Å^{-1}$, and $c^0_{PIP_2} = 1/70\ Å^{-1}$ (see the Supporting Material). For both calculations, the BAR dimer was fixed in space as depicted in Fig. 1, *B* and *C*. (*A–D*) Equilibrium shapes of PIP_2/PC and PS/PC membranes, respectively, with contours shown for the local heights of the upper and lower leaflets. (*E–H*) Steady-state lipid distributions on upper and lower leaflets in both membranes. The color code for the contour plots is the same as in Fig. 1 *C*, and color shades for panels *E–H* represent ratios of local and average lipid fraction values.

a greater extent than monovalent lipids at the steady state, is consistent with our own and the previous calculations of others and with experiments (27,45–47,60–62), and has been attributed mainly to the smaller lipid demixing penalty associated with segregating polyvalent PIP_2 lipids than monovalent PS. Interestingly, the lipid demixing on the lower leaflets of both membranes, shown in Fig. 2, *F* and *H*, can be explained entirely by bending forces forming regions depleted in PS and PIP_2 lipid in the regions of negative curvatures (*yellow shades*).

We find that the adsorption free energies ΔF (see the Supporting Material) for the BAR onto PS-containing membranes is $-7.2\ k_BT$, and $-5.3\ k_BT$ for PIP_2-containing membranes, relative to the states where BAR is infinitely separated from a flat membrane with corresponding homogeneous lipid distribution. BAR binds more efficiently to the $\phi_{PS} = 0.3$ compared to $\phi_{PIP_2} = 0.04$ bilayer because of the higher average surface charge density of the PS-containing patch. Lipid demixing and membrane deformations further contribute to lowering ΔF for BAR/PS/PC and BAR/PIP_2/PC complexes by ~1.9 k_BT and ~1.7 k_BT, respectively, compared to the binding free energies of BAR onto the flat PS/PC and PIP_2/PC membranes of the same homogeneous compositions. Nevertheless, from Fig. 2, it is clear that the combination of lipid segregation with the elastic forces within a membrane is still insufficient to produce significant compositional asymmetry between bilayer leaflets. Consequently, at steady state, the membrane remains near-flat, within fluctuations, upon BAR adsorption.

N-helix insertions can potentially enhance membrane deformations

Results in the previous section suggest that for a single BAR to bend a membrane significantly, the asymmetry between monolayers must originate from additional energy sources that were not within the free energy function to this point. One such mechanism is the prior insertions of the BAR dimer's N-helices. Generally, inclusion of an amphipathic peptide into one of the leaflets of a flat membrane can result in local spontaneous curvature regions in the bilayer (14,26,63). The magnitude of the spontaneous curvature has been predicted to depend on the insertion depth, with c_0-values ranging from 0 to 0.05 $Å^{-1}$ (26,63).

Results from including effects of N-helix insertions in the calculations (see the Supporting Material) are presented in Fig. 3, showing equilibrium membrane contours for bilayers with different bending rigidities and different spontaneous

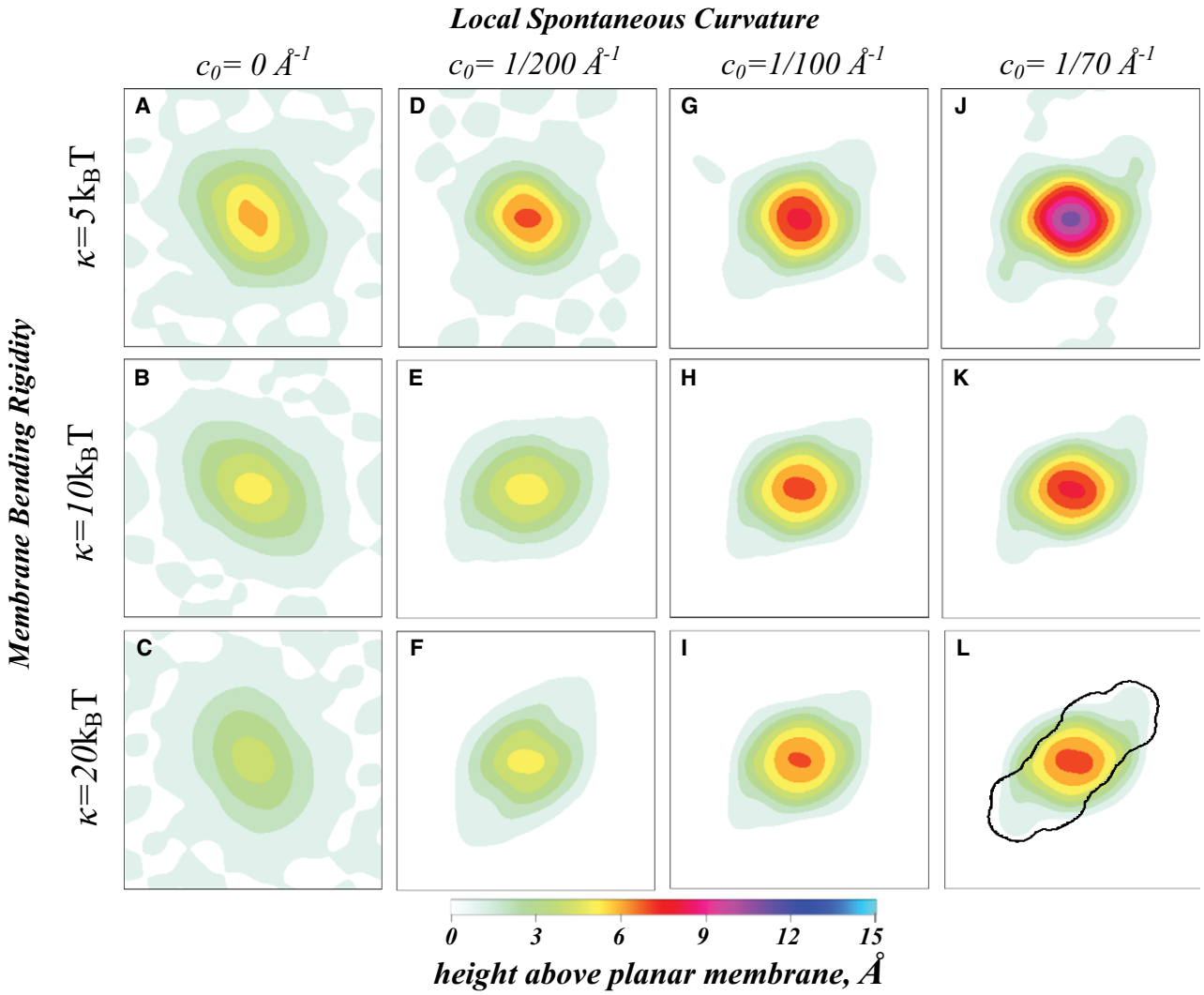

FIGURE 3 Color online only. Steady-state shapes plotted as upper leaflet contours of membranes with different bending rigidities and with N-helix insertions of various depths upon binding of the Amphiphysin N-BAR domain dimer. The membrane patches have $\sigma = -0.004e/\text{Å}^2$ average surface charge densities ($\phi^0_{PS} = 0.3$) on both layers, and BAR is oriented in the same way as in Fig. 1, *B* and *C*. We consider bilayers with bending rigidities $\kappa = 20\ k_BT$ (*lower panels*), $\kappa = 10\ k_BT$ (*middle panels*), and $\kappa = 5\ k_BT$ (*upper panels*). For all systems, a nonzero spontaneous curvature domain is defined for a membrane patch inside the BAR projection area shown in Fig. 1 *C* and extending 20 Å away from the projected zone. For clarity, the border of one such nonzero spontaneous curvature domain is shown as a black contour in panel *L*. We consider $c_0 = 0$ Å^{-1} (*A–C*), 1/200 Å^{-1}(*D–F*), 1/100 Å^{-1} (*G–I*), or 1/70 Å^{-1} (*J–L*) for the bilayer region inside this contour, and $c_0 \rightarrow 0$ with exponential decay outside.

curvatures assigned to the BAR underlying regions. These correspond to the possible curvatures resulting from insertion parameters, e.g., various penetration depths. For this set of calculations, we consider membranes with average surface charge densities of $\sigma = -0.004e/\text{Å}^2$, which corresponds, for example, to $\phi_{PS} = 0.3$. The effect of the N-BAR helix insertion is modeled implicitly by defining a membrane area of nonzero spontaneous curvature (*black contour* in Fig. 3 *L*) that lies under the BAR projection area (shown in Fig. 1 *C*) and extends 20 Å around this projected region. The size of this peptide-membrane interaction zone is consistent with the results of Zemel et al. (63), showing that the effect of peptide insertion on lipid packing extends to a distance of ~15–20 Å. Within this domain, we have allowed the membrane to adopt different curvatures ranging from $c_0 = 0$ Å^{-1} (Fig. 3, *A–C*), through 1:200 Å^{-1} (Fig. 3, *D–F*), 1:100 Å^{-1} (Fig. 3, *G–I*), and to 1:70 Å^{-1} (Fig. 3, *J–L*); all c_0-values are taken at the bilayer midplane, and c_0 rapidly decays to zero outside the interaction zone. Although from our model we cannot specify the exact insertion depths to which these c_0 values would correspond, using the results from Campelo et al. (26), it is reasonable to estimate that the interval of c_0-values used here will best describe N-helix penetration depths in the range of 0–2.5 Å into the upper leaflet surface.

To investigate how membranes of different rigidities respond to possible N-helix insertions and electrostatic forces exerted by the adsorbing BAR, we also consider bilayers of different stiffness by varying the bending modulus κ.

Equilibrium states are calculated for membranes with a commonly encountered rigidity value of $\kappa = 20\ k_BT$ (*lower panels*), intermediate rigidity $\kappa = 10\ k_BT$ (*middle panels*), and soft bilayers $\kappa = 5\ k_BT$ (*upper panels*), all κ-values taken here per bilayer (κ-value representing the soft bilayers generally describes thin membranes, or ones with added short-chain co-surfactants (64–67)). A homogeneous and constant lipid distribution is assumed based on the results in Fig. 2, suggesting that segregation of charged lipids under the adsorbing BAR is minimal.

The results (Fig. 3) reveal two general trends: The first is that at equilibrium, softer membranes show more prominent bilayer deformations, as more significant values of bending are reached with increasing c_0. Table 1 summarizes the highest contour levels, h_{max}. From Eq. 8, the magnitudes of membrane deformations for $c_0 = 1/100$ Å^{-1} and 1/70 Å^{-1} systems are beyond the predicted range of undulations for all the bending moduli, making them substantial with respect to thermal fluctuations. The largest calculated local deformations range from $h_{max} = 11$ Å for $\kappa = 5\ k_BT$ and $c_0 = 1/70$ Å^{-1} membrane to $h_{max} = 7$ Å for $\kappa = 20\ k_BT$ and $c_0 = 1/70$ Å^{-1} patch (see Table 1 and Fig. 3).

Interestingly, although the strongest deformations are found for membranes with the largest c_0 corresponding to the deepest N-helical insertions(Fig. 3, *J–L*), the results for adsorption free energies (Fig. 4) suggest that the BAR appears to thermodynamically stabilize most effectively bilayers with $c_0 = 1/100$ Å^{-1}. Fig. 4 shows the binding free energies (in k_BT units) that relate to BAR-membrane interactions beyond the initial N-helical penetration, i.e., the gain in free energy that is achieved by BAR adsorption, but excluding contributions from the amphipathic helix insertions. Remarkably, the c_0-value corresponding to the minimum free energy is very close to the intrinsic radius of curvature of the membrane-facing side of the Amphyphysin BAR itself, of ~110 Å (10). Thus, we predict that a single BAR domain will most effectively stabilize a membrane region where preceding N-helical insertions have locally created spontaneous curvature that closely matches the radius of curvature of the BAR domain itself.

TABLE 1 Largest membrane deformation levels, h_{max}, for patches shown in Fig. 3

κ, k_BT	c_0, Å^{-1}	h_{max}, Å
5	0	6
	1/200	7
	1/100	8
	1/70	11
10	0	5
	1/200	5
	1/100	7
	1/70	8
20	0	4
	1/200	5
	1/100	7
	1/70	7

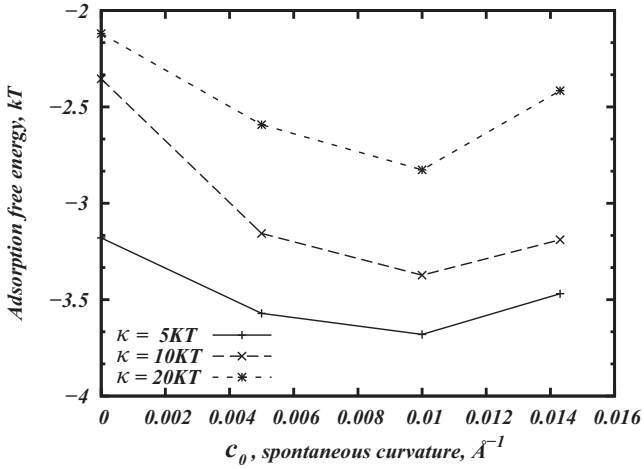

FIGURE 4 Gains in the adsorption free energies (in k_BT units) for the BAR-membrane parameters described in Fig. 3 pertaining to the BAR/membrane interactions after the initial N-helix penetration.

The role of electrostatic interactions in stabilization

We varied the homogeneous surface charge densities for the patches shown in Fig. 3, and the free energy minimization (data not shown) revealed that doubling the magnitude of σ from –0.004e/Å^2 to –0.008e/Å^2, corresponding to varying the PS composition in PS/PC membrane from $\phi^0_{PS} = 0.3$–0.5, resulted in stronger binding with substantial change in ΔF (~6 k_BT) without noticeable changes in the equilibrium membrane deformation shown in Fig. 3. Thus, we conclude that the electrostatic interactions are critical to the stabilization of the BAR-membrane complex after the initial N-helix insertions.

BAR as a curvature sensor

So far, a single BAR domain was considered to adsorb onto spontaneously flat membranes. Because BAR has been suggested to play a crucial role not only as a curvature generator, but also as a sensor of high curvature regions on cell membranes and vesicles (14,68), we investigate this aspect of BAR-membrane interactions by having the BAR bind to membranes that are already bent. The binding free energy calculations were done with lipid bilayers of $\sigma = -0.004e$/Å^2 surface charge density ($\phi_{PS} = 0.3$) and a homogeneous lipid distribution with a simplified spherical cap deformation. The results are shown in Fig. S1 in the Supporting Material, which depicts the adsorption free energy versus the radius of the spherical cap R. A range of R from 800 Å (near flat membrane) to 100 Å (closely matching BAR's intrinsic shape) was considered. In the reference state for these calculations BAR is infinitely separated from a membrane that has the same spherical deformation as it does when complexed with BAR, so that, unlike our previous calculations, the adsorption free energies in Fig. S1 do not contain elastic contributions.

We find that BAR adsorbs preferentially on membranes of high curvature (low R), and the difference in the binding free energies between membranes with $R = 800$ Å and $R = 100$ Å

is substantial at 7.7 k_BT. This can be explained based on two considerations: First, when BAR adsorbs on bent bilayers, there is no free energy cost associated with membrane deformation that has to be overcome. Second, through the positively charged residues on its concave surface, the BAR dimer more efficiently minimizes the electrostatic interactions with bent membranes compared to the relatively flat one (see Fig. 1). Thus, our results indicate that the BAR dimer can sense bilayer regions of high curvature through electrostatic interactions with the membrane.

DISCUSSION

The illustration of our method by application to the quantitative modeling of a single Amphyphysin BAR domain interacting with large patches of lipid membrane bilayers of heterogeneous compositions has produced some novel insights into membrane remodeling mechanisms. Thus, our calculations predict that a single BAR dimer is capable of producing an equilibrium state, in which the initially near-planar membrane curves significantly. This is consistent with results from atomistic MD simulations (24,25). The results indicate further that the deformations required for these interactions occur only for membrane patches that have the propensity to attain high spontaneous curvature. Such favorable membrane preconditioning may be the result of N-helix insertions, but cannot be produced by local segregation of monovalent or even polyvalent lipids. Thus, we conclude that N-helix insertions may have a critical mechanistic role in the function of BAR domains. We show further that the electrostatic interactions are essential for sensing and stabilization of existing bilayer curvature. Finally, we predict that a single BAR will most efficiently stabilize a membrane region where preceding N-helix insertions create locally a spontaneous curvature that closely matches the radius of curvature of the BAR itself. Clearly, some of the inferences drawn from the application of our method to the Amphiphysin BAR domain may be characteristic for this specific protein. The generality will be tested by the application to other, structurally diverse BAR domains, which is currently underway.

The good agreement between the results obtained with our methods and the previous findings from MD simulations (25) suggests that N-BAR domains that do not have their amphipathic helices embedded in the bilayer, do not induce curvature. In further agreement with Blood et al., we also find that electrostatic interactions are essential for bilayer curvature stabilization. Interestingly, Blood et al. (25) suggests that increased amounts of PIP_2 lipids in the patch immediately underneath the BAR results in stronger binding of the N-BAR even without helix insertions. This conclusion seemingly contradicts our model's predictions (see Fig. 2), but we note that the inference in Blood et al. (25) is based on the MD simulations of N-BAR adsorbing onto ternary ~70:30:1 PC/PS/PIP_2 membrane, where PIP_2 lipids, by construction, were not initially dispersed randomly, but rather were localized near the BAR with a local concentration reaching ~10%. Our model, on the other hand, predicts that starting from a homogeneous 96:4 PC/PIP_2 distribution, PIP_2 lipid levels beneath the adsorbed BAR at steady state, after lipids are allowed to diffuse in the membrane plane, reach only ~5% (Fig. 2). Obviously, the presence of PS lipids in the system will only lower this number (27).

In considering this apparent discrepancy, one must keep in mind that the method presented here obtains the sequestered levels of PIP_2 from a self-consistent equilibrium calculation, whereas it is not clear whether the PIP_2 lipid distribution used in Blood et al. (25) corresponds to the same steady-state solution, or to an another intermediate configuration.

Our results offer additional insights regarding the effect of a single BAR dimer's interaction with the membrane. Fig. 3 shows that, upon BAR adsorption, bilayers with $c_0 = 0$ Å^{-1}, corresponding to no peptide penetrations, achieve minimization of intramembrane elastic forces by curving in the direction perpendicular to the BAR long axis (Fig. 1 *C*). This mechanism is possible because lipid molecules on both sides of the BAR projection-zone are less engaged in electrostatic interactions with the BAR compared to lipids directly under BAR (see also Fig. 2), and thus are less constrained in readjusting their positions so as to minimize the bending energy. Conversely, if N-helix inclusions create locally nonzero spontaneous curvatures, the model predicts curving along the BAR major axis. Importantly, for all systems in Figs. 2 and 3, our calculations clearly show that BAR binding results in symmetry breaking so that equilibrium membrane shapes predicted from the model are strongly anisotropic. In quantitative terms, one can obtain local curvature values in principal directions, along ($c_{\|}$) and perpendicular ($c_{\perp}$) to the BAR major axis, for the membrane region directly underneath the BAR. As an example, the two curvatures at the highest membrane deformation area (at the bilayer center) for $\kappa = 20\ k_BT$ and $c_0 = 0$ Å^{-1} system (Fig. 3 *C*) are $c_{\|} = 0.0053$ Å^{-1}, and $c_{\perp} = 0.0006$ Å^{-1}, but for $\kappa = 20\ k_BT$ and $c_0 = 1/70$ Å^{-1} system (Fig. 3 *L*) we find $c_{\|} = 0.0068$ Å^{-1}, and $c_{\perp} = 0.0035$ Å^{-1}, consistent with the observed curvature directionality change.

Symmetry breaking upon BAR adsorption was observed as well in the atomistic simulations (24,25), and in mesoscale theoretical studies (22,23), and demonstrated experimentally in terms of formation of striations on remodeled tubes (1,2). We stress that, like all other features predicted from our model, the observed symmetry breaking and resulting anisotropic local curvatures result from the self-consistent free energy minimization, without a priori assumption of any BAR-induced spontaneous curvature fields. The approach is somewhat different from that developed in Ayton et al. (23), where the authors treat BAR-membrane interactions implicitly, through either assumed isotropic or anisotropic spontaneous curvature fields generated by adsorbed N-BARs. Within this formalism, Ayton et al. observe membrane tubulation when they consider anisotropic spontaneous curvature

fields of BAR-membrane complexes in the Helfrich free energy expression (23), whereas vesiculation is obtained for isotropic spontaneous curvature fields but for high N-BAR densities. In fact, the measure that we find for BAR-membrane complex curvature could be interpreted as the spontaneous curvature of the BAR-membrane complex. This value should not be confused with c_0 of the bare membrane, and will generally also depend on the density of BARs on the membrane. The values presented here are applicable in the low BAR density limit.

A question that remains open is how the observed local deformations introduced by a single BAR translate into global changes in membrane shape observed upon binding of high concentrations of BARs. Arkhipov et al. (22) suggest that BAR modules achieve membrane reshaping in a two-row staggered arrangement, but fail to do so when aligned in one line. Results of our calculations (Fig. 3) predict that, as a result of interplay between electrostatic and elastic forces, a single BAR dimer deforms membranes so that the bilayer region under the BAR can be substantially curved. At the same time, the membrane remains flat within fluctuations beyond this interaction zone. Thus, it is clear that surrounding this high curvature area there must exist a narrow region, a rim, where the sign of the local membrane curvature changes from positive (under the BAR) to negative (outside the interaction zone) eventually decaying to zero. Although electrostatically advantageous, the formation of such a rim is opposed by bending forces within a membrane, since lipids inside the rim pay an elastic penalty for bending away from c_0. The larger the membrane deformations, the larger the free energy penalty exerted on the rim. Therefore, we conclude that binding of an additional BAR will be most favorable energetically if, together with minimizing the electrostatic interactions, the BAR also alleviates the membrane stress introduced by the one already adsorbed. The optimal manner for achieving this effect with multiple BARs is clearly not a simple additive superposition of effects from a single BAR. Systems in which large arrays of BAR domain dimers were shown to produce tubulation with membrane-specific and BAR-specific properties (1,2,22) exhibit symmetry and other attributes that bespeak collective properties. Such mechanisms will be addressed with the next extension of our model.

SUPPORTING MATERIAL

Sixteen equations and supporting text are available at http://www.biophysj.org/biophysj/supplemental/S0006-3495(09)01213-2.

Computational resources of the David A. Cofrin Center for Biomedical Information in the HRH Prince Alwaleed Bin Talal Bin Abdulaziz Alsaud Institute for Computational Biomedicine are gratefully acknowledged.

The work was supported by grants from the National Institutes of Health (No. P01 DA012408 and No. P01 DA012923, to G.K. and H.W.). D.H. is supported by the Israeli Council of Higher Education through an Alon Fellowship, as well as a Career Development Award from the Hebrew University Intramural Research Fund. The Fritz Haber Research Center is supported by the Minerva Foundation, Munich, Germany.

REFERENCES

1. Frost, A., R. Perera, A. Roux, K. Spasov, O. Destaing, et al. 2008. Structural basis of membrane invagination by F-BAR domains. *Cell.* 132:807–817.
2. Shimada, A., H. Niwa, K. Tsujita, S. Suetsugu, K. Nitta, et al. 2007. Curved EFC/F-BAR-domain dimers are joined end to end into a filament for membrane invagination in endocytosis. *Cell.* 129:761–772.
3. Saarikangas, J., H. Zhao, A. Pykalainen, P. Laurinmaki, P. K. Mattila, et al. 2009. Molecular mechanisms of membrane deformation by I-BAR domain proteins. *Curr. Biol.* 19:95–107.
4. Ren, G., P. Vajjhala, J. S. Lee, B. Winsor, and A. L. Munn. 2006. The BAR domain proteins: molding membranes in fission, fusion, and phagy. *Microbiol. Mol. Biol. Rev.* 70:37–120.
5. Habermann, B. 2004. The BAR-domain family of proteins: a case of bending and binding? *EMBO Rep.* 5:250–255.
6. Dawson, J. C., J. A. Legg, and L. M. Machesky. 2006. BAR domain proteins: a role in tubulation, scission and actin assembly in clathrin-mediated endocytosis. *Trends Cell Biol.* 16:493–498.
7. Perez, J. L., L. Khatri, C. Chang, S. Srivastava, P. Osten, et al. 2001. PICK1 targets activated protein kinase Cα to AMPA receptor clusters in spines of hippocampal neurons and reduces surface levels of the AMPA-type glutamate receptor subunit 2. *J. Neurosci.* 21:5417–5428.
8. Lu, W., and E. B. Ziff. 2005. PICK1 interacts with ABP/GRIP to regulate AMPA receptor trafficking. *Neuron.* 47:407–421.
9. Jin, W., W.-P. Ge, J. Xu, M. Cao, L. Peng, et al. 2006. Lipid binding regulates synaptic targeting of PICK1, AMPA receptor trafficking, and synaptic plasticity. *J. Neurosci.* 26:2380–2390.
10. Peter, B. J., H. M. Kent, I. G. Mills, Y. Vallis, P. J. G. Butler, et al. 2004. BAR domains as sensors of membrane curvature: the Amphiphysin BAR structure. *Science.* 303:495–499.
11. Madsen, K. L., J. Eriksen, L. Milan-Lobo, D. S. Han, M. Y. Niv, et al. 2008. Membrane localization is critical for activation of the PICK1 BAR (Bin/amphiphysin/Rvs) domain. *Traffic.* 9:1327–1343.
12. Gallop, J. L., and H. T. McMahon. 2005. BAR domains and membrane curvature: bringing your curves to the BAR. *Biochem. Soc. Symp.* 72:223–231.
13. Itoh, T., and P. De Camilli. 2006. BAR, F-BAR (EFC) and ENTH/ANTH domains in the regulation of membrane-cytosol interfaces and membrane curvature. *Biochim. Biophys. Acta.* 1761:897–912.
14. Zimmerberg, J., and M. M. Kozlov. 2006. How proteins produce cellular membrane curvature. *Nat. Rev. Mol. Cell Biol.* 7:9–19.
15. Gallop, J. L., C. C. Jao, H. M. Kent, P. J. G. Butler, P. R. Evans, et al. 2004. Mechanism of endophilin N-BAR domain-mediated membrane curvature. *EMBO J.* 25:2898–2910.
16. Farsad, K., N. Ringstad, K. Takei, S. R. Floyd, K. Rose, et al. 2001. Generation of high curvature membranes mediated by direct endophilin bilayer interactions. *J. Cell Biol.* 155:193–200.
17. Masuda, M., S. Takeda, M. Sone, T. Ohki, H. Mori, et al. 2006. Endophilin BAR domain drives membrane curvature by two newly identified structure-based mechanisms. *EMBO J.* 25:2889–2897.
18. Ford, M. G. J., I. G. Mills, B. J. Peter, Y. Valls, G. J. K. Praefcke, et al. 2002. Curvature of clathrin-coated pits driven by epsin. *Nature.* 419:361–366.
19. Lee, M. C. S., L. Orci, S. Hamamoto, E. Futal, M. Ravazzola, et al. 2005. Sar1p N-terminal helix initiates membrane curvature and completes the fission of a COPII vesicle. *Cell.* 122:605–617.
20. Nie, Z., D. S. Hirsch, R. Luo, X. Jian, S. Stauffer, et al. 2006. A BAR domain in the N terminus of the Arf GAP ASAP1 affects membrane structure and trafficking of epidermal growth factor receptor. *Curr. Biol.* 16:130–139.
21. Fernandes, F., L. M. S. Loura, F. J. Chichon, J. L. Carrascosa, A. Fedorov, et al. 2008. Role of helix-0 of the N-BAR domain in membrane curvature generation. *Biophys. J.* 94:3065–3073.
22. Arkhipov, A., Y. Yin, and K. Schulten. 2008. Four-scale description of membrane sculpting by BAR domains. *Biophys. J.* 95:2806–2821.

23. Ayton, G. S., P. D. Blood, and G. A. Voth. 2007. Membrane remodeling from N-BAR domain interactions: insights from multi-scale simulation. *Biophys. J.* 92:3595–3602.
24. Blood, P. D., and G. A. Voth. 2006. Direct observation of Bin/Amphiphysin/Rvs (BAR) domain-induced membrane curvature by means of molecular dynamics simulations. *Proc. Natl. Acad. Sci. USA.* 103:15068–15072.
25. Blood, P. D., R. D. Swenson, and G. A. Voth. 2008. Factors influencing local membrane curvature induction by N-BAR domains as revealed by molecular dynamics simulations. *Biophys. J.* 95:1866–1876.
26. Campelo, F., H. T. McMahon, and M. M. Kozlov. 2008. The hydrophobic insertion mechanism of membrane curvature generation by proteins. *Biophys. J.* 95:2325–2339.
27. Khelashvili, G., H. Weinstein, and D. Harries. 2008. Protein diffusion on charged membranes: a dynamic mean-field model describes time evolution and lipid reorganization. *Biophys. J.* 94:2580–2597.
28. Harries, D., S. May, and A. Ben-Shaul. 2003. Curvature and charge modulations in lamellar DNA-lipid complexes. *J. Phys. Chem. B.* 107:3624–3630.
29. Helfrich, W. 1973. Elastic properties of lipid bilayers: theory and possible experiments. *Z. Naturforsch. [C].* 28c:693–703.
30. Sharp, K. A., and B. Honig. 1990. Electrostatic interactions in macromolecules: theory and applications. *Annu. Rev. Biophys. Chem.* 19:301–332.
31. Andelman, D. 1995. Electrostatic properties of membranes: the Poisson-Boltzmann theory. *In* Handbook of Biological Physics. Elsevier Science, Amsterdam, The Netherlands.
32. Reiner, E. S., and C. J. Radke. 1990. Variational approach to the electrostatic free energy in charged colloidal suspensions: general theory for open systems. *J. Chem. Soc., Faraday Trans.* 86:3901–3912.
33. Honig, B., and A. Nicholls. 1995. Classical electrostatics in biology and chemistry. *Science.* 268:1144–1149.
34. Borukhov, I., D. Andelman, and H. Orland. 1997. Steric effects in electrolytes: a modified Poisson-Boltzmann equation. *Phys. Rev. Lett.* 79:435–438.
35. Fogolari, F., and J. M. Briggs. 1997. On the variational approach to the Poisson-Boltzmann free energies. *Chem. Phys. Lett.* 281:135–139.
36. Murray, D., A. Arbuzova, B. Honig, and S. McLaughlin. 2002. The role of electrostatic and nonpolar interactions in the association of peripheral proteins with membranes. *Curr. Topics Membr.* 52:277–307.
37. Chernomordik, L. V., and M. M. Kozlov. 2003. Protein-lipid interplay in fusion and fission of biological membranes. *Annu. Rev. Biochem.* 72:175–207.
38. Jahn, R., and H. Grubmuller. 2002. Membrane fusion. *Curr. Opin. Cell Biol.* 14:488–495.
39. Kozlovsky, Y., A. Efrat, D. A. Siegel, and M. M. Kozlov. 2004. Stalk phase formation: effects on dehydration and saddle splay modulus. *Biophys. J.* 87:2508–2521.
40. Kozlovsky, Y., and M. M. Kozlov. 2003. Membrane fission: model for intermediate structures. *Biophys. J.* 85:85–96.
41. Wiese, W., and W. Helfrich. 1990. Theory of vesicle budding. *J. Phys. Condens. Matter.* 2:SA329–SA332.
42. Mashl, R. J., and R. F. Bruinsma. 1998. Spontaneous-curvature theory of clathrin-coated membranes. *Biophys. J.* 74:2862–2875.
43. May, S., D. Harries, and A. Ben-Shaul. 2000. Lipid demixing and protein-protein interactions in the adsorption of charged proteins on mixed membrane. *Biophys. J.* 79:1747–1760.
44. Harries, D., S. May, W. M. Gelbart, and A. Ben-Shaul. 1998. Structure, stability, and thermodynamics of lamellar DNA-lipid complexes. *Biophys. J.* 75:159–173.
45. Haleva, E., N. Ben-Tal, and H. Diamant. 2004. Increased concentration of polyvalent phospholipids in the adsorption domain of a charged protein. *Biophys. J.* 86:2165–2178.
46. Wang, J., A. Gambhir, S. McLaughlin, and D. Murray. 2004. A computational model for the electrostatic sequestration of $PI(4,5)P_2$ by membrane-adsorbed based peptides. *Biophys. J.* 86:1969–1986.
47. McLaughlin, S., and D. Murrray. 2005. Plasma membrane phosphoinositide organization by protein electrostatics. *Nature.* 438:605–611.
48. Hill, T. L. 1987. An Introduction to Statistical Thermodynamics. Dover Publications, Mineola, NY.
49. Kozlov, M. M., and M. Winterhalter. 1991. Elastic moduli and neutral surface for strongly curved monolayers. Analysis of experimental results. *J. Phys. II* (*Fr.*) 1:1085–1100.
50. Funkhouser, C. M., F. J. Solis, and K. Thornton. 2007. Coupled composition-deformation phase-field method for multicomponent lipid membranes. *Phys. Rev. E.* 76:011912(15).
51. Andelman, D., M. M. Kozlov, and W. Helfrich. 1994. Phase transitions between vesicles and micelles driven by competing curvature. *Europhys. Lett.* 25:231–236.
52. Fournier, J. B. 1996. Nontopological saddle-splay and curvature instabilities from anisotropic membrane inclusions. *Phys. Rev. Lett.* 76:4436–4439.
53. Petrache, H. I., D. Harries, and V. A. Parsegian. 2005. Alteration of lipid membrane rigidity by cholesterol and its metabolic precursors. *Macromol. Symp.* 219:39–50.
54. Petrache, H. I., N. Gouliaev, S. Tristram-Nagle, R. T. Zhang, R. M. Sutter, et al. 1998. Interbilayer interactions from high-resolution x-ray scattering. *Phys. Rev. E Stat. Phys. Plasmas Fluids Relat. Interdiscip. Topics.* 57:7014–7024.
55. Evans, E. A., and V. A. Parsegian. 1986. Thermal-mechanical fluctuations enhance repulsion between biomolecular layers. *Proc. Natl. Acad. Sci. USA.* 83:7132–7136.
56. Podgornik, R., and V. A. Parsegian. 1992. Thermal-mechanical fluctuations of fluid membranes in confined geometries: the case of soft confinement. *Langmuir.* 8:557–562.
57. Chaikin, P. M., and T. C. Lubensky. 2000. Principles of Condensed Matter Physics. Cambridge University Press, Cambridge, UK.
58. Lipowsky, R., and E. Sackmann. 1995. Structure and Dynamics of Membranes. Elsevier, Amsterdam, The Netherlands.
59. Lindahl, E., and O. Edholm. 2000. Mesoscopic undulations and thickness fluctuations in lipid bilayers from molecular dynamics simulations. *Biophys. J.* 79:426–433.
60. Wang, J., A. Gambhir, G. Hangyas-Mihalyne, D. Murray, U. Golebiewska, et al. 2002. Lateral sequestration of phosphatidylinositol 4,5-biphosphate by the basic effector domain of myristoylated alanine-rich C Kinase substrate is due to nonspecific electrostatic interactions. *J. Biol. Chem.* 277:34401–34412.
61. Golebiewska, U., A. Gambhir, G. Hangyas-Mihalyne, I. Zaitseva, J. Radler, et al. 2006. Membrane-bound basic peptides sequester multivalent (PIP_2), but not monovalent (PS), acidic lipids. *Biophys. J.* 91:588–599.
62. Tzlil, S., and A. Ben-Shaul. 2004. Increased concentration of polyvalent phospholipids in the adsorption domain of a charged protein. *Biophys. J.* 89:2165–2178.
63. Zemel, A., A. Ben-Shaul, and S. May. 2005. Perturbation of a lipid membrane by amphiphatic peptides and its role in pore formation. *Eur. Biophys. J.* 34:230–242.
64. Danino, D., E. Kesselman, G. Saper, H. I. Petrache, and D. Harries. *Biophys. J.* In press.
65. Pabst, G., S. Danner, R. Podgornik, and J. Katsaras. 2007. Entropy-driven softening of fluid lipid bilayers by alamethicin. *Langmuir.* 23:11705–11711.
66. Safinya, C. R., E. B. Sirota, D. Roux, and G. S. Smith. 1989. Universality in interacting membranes: the effect of cosurfactants on the interfacial rigidity. *Phys. Rev. Lett.* 62:1134–1137.
67. Kozlov, M. M., and W. Helfrich. 1992. Effects of a cosurfactant on the stretching and bending elasticities of a surfactant monolayer. *Langmuir.* 8:2792–2797.
68. McMahon, H. T., and J. L. Gallop. 2005. Membrane curvature and mechanisms of dynamic cell membrane remodeling. *Nature.* 438: 590–596.

Supporting Material

"Modeling membrane deformations and lipid demixing upon protein-membrane interaction: The BAR dimer adsorption"

George Khelashvili, Daniel Harries, and Harel Weinstein

Parametrization of Membrane Shape

In this section we present the parametrization procedure for the membrane shape. Our description is based on the Monge representation where a position vector $\vec{r}$ of the bilayer upper or lower leaflets, or bilayer mid-plane (see Fig. $1B$ of the main text) is given by $\vec{r} \equiv (x, y, h(x, y))$. The height function $h(x, y)$ is the distance between the curved surface and the flat reference (x, y) plane. In the Monge gauge the metric of the surface is given by:

$$g_{ij} = \frac{\partial \vec{r}}{\partial u^i} \times \frac{\partial \vec{r}}{\partial u^j}, \qquad i, j = 1, 2 \tag{1}$$

where $u^1 \equiv x, u^2 \equiv y$. From Eq. 1

$$g \equiv |g_{ij}| = 1 + h_x^2 + h_y^2 \tag{2}$$

with $h_x \equiv \partial_x h(x, y)$ and $h_y \equiv \partial_y h(x, y)$. The area element of the curved surface is:

$$dA = \sqrt{g} dx dy = \sqrt{1 + h_x^2 + h_y^2} dx dy \tag{3}$$

and the Cartesian components of the local surface element normal unit vector $\vec{n} = (n_x, n_y, n_z)$ are given by:

$$n_x = \frac{-h_x}{\sqrt{g}} \tag{4}$$

$$n_y = \frac{-h_y}{\sqrt{g}} \tag{5}$$

$$n_z = \frac{1}{\sqrt{g}} \tag{6}$$

With that, one can derive for the local curvature:

$$c(x, y) = \frac{(1 + h_y^2) h_{xx} + (1 + h_x^2) h_{yy} - 2 h_x h_y h_{xy}}{2 g^{3/2}} \tag{7}$$

where $h_{xx} \equiv \partial_{xx} h(x,y)$, $h_{yy} \equiv \partial_{yy} h(x,y)$, and $h_{xy} \equiv \partial_{xy} h(x,y)$. Eq. 3 and Eq. 7 are used throughout the equations in the main text and in the Supporting Material.

Elements of membrane remodeling

In the transformation of a membrane that is spontaneously flat at equilibrium into a highly curved structure, BAR appears to take advantage of a special set of structural features. First, the electrostatic interactions between positively charged residues on BAR's concave surface and phospholipid headgroups may cause membrane deformations out of the bilayer plane, resulting in a pulling of the membrane towards, or away from the protein. The same electrostatic interactions may also cause lateral sequestration of charged phospholipids near the protein(1–7). This process of lipid demixing in the bilayer plane has been predicted to be particularly significant in membranes containing multivalent lipids, such as phosphatidylinositol 4,5-biphosphate (PIP_2) lipids(1, 3). Segregation of such highly charged lipids (net head-group charge of -4.0 at neutral pH(8)) would not only enhance the overall electrostatic interactions between BAR and membrane, but could lead as well to local asymmetry between the spontaneous curvatures of the two monolayers comprising a lipid membrane, simply because the head group of PIP_2 is larger than most mono-valent lipids, such as phosphatidylserine (PS) or zwiterionic lipids, like phosphatidylcholine (PC). Such asymmetry would be sufficient to produce a local "positive" curvature in the two *bilayer* leaflets, towards the BAR(9–11). Therefore, sequestering charged lipids could potentially lead to a new stable state, in which bilayer bending forces favor membranes with local non-zero curvature.

These components of the interaction energy are accounted for in the approach we describe here. Moreover, the mechanism for coupling local

lipid composition with membrane curvature may be complemented by a "local spontaneous curvature" mechanism (11), in which the asymmetry between the spontaneous shapes of two monolayers is achieved by insertion of amphipathic N-terminal helices of certain BAR domains into the lipids polar headgroups region(11–21). In this mechanism, the insertion of an amphipathic peptide into one of the leaflets of a flat membrane produces an increase in the local spontaneous curvature of that leaflet because of the local bending of the monolayer where the helix is embedded(9–11). Differences in the spontaneous curvatures of two monolayers comprising a lipid membrane establishes a new equilibrium state, in which, bilayer elastic forces support a locally curved membrane shape.

Free energy minimization

In this section we detail the free energy minimization procedure implemented to obtain an equilibrium state for BAR-membrane complex. Because the free energy functional F (Eq.(2) of the main text) contains electrostatic, mobile ion mixing, lipid mixing, and membrane bending energy contributions, F must be minimized with respect to all these relevant degrees of freedom in a self-consistent manner. In particular, minimization with respect to mobile ion concentrations leads to the non-linear Poisson-Boltzmann (PB) equation(22–28):

$$\nabla^2\Psi = \lambda_D^{-2}\sinh\Psi \tag{8}$$

Solving this equation yields the electrostatic potential Ψ.

In order to minimize the free energy functional with respect to the lipid compositional degrees of freedom, we use the Cahn-Hilliard (CH) formalism (29), carried out here as discussed in detail in Ref.(1). Briefly, according to the CH description, lipids diffuse in the membrane plane due to the local

gradients in their electrochemical potentials(30, 31), where the steady-state solution of the CH equations at long times is obtained self-consistently with the PB equation and corresponds to the lipid distribution that minimizes F with respect to all local lipid mole fractions. Thus, propagating local lipid compositions with these diffusion-like equations eliminates the need to tackle an additional 2D boundary condition on the membrane surface(1, 32, 33), which in general is easily solvable only for systems of high geometric symmetry.

In order to implement the CH formalism for a membrane composed of binary mixtures of charged and neutral lipids, we first use free energy functional expression (Eq.(2) of the main text) to derive the electrochemical potential of charged lipids on either leaflet as:

$$\mu = \mu^{\circ} + \frac{\partial F}{\partial N} = \mu^{\circ} + k_B T \left[\ln \frac{\phi(1-\phi^0)}{\phi^0(1-\phi)} + z\Psi \right] + a\kappa(c_n^0 - c_c^0)(c - c^0(\phi)) \quad (9)$$

Here N is the number of charged lipids on a single membrane layer, and μ° represents the standard chemical potential for the charged lipid species(that is independent of ϕ). The temporal evolution of the spatial charged-lipid compositions on both leaflets are linked to the Laplacians of the corresponding electrochemical potentials through the pair of CH equations:

$$\begin{aligned} \frac{\partial \phi_u(\vec{r},t)}{\partial t} &= \frac{D_{lip}}{k_B T} \nabla^2_{LB}(\mu_u) \\ \frac{\partial \phi_l(\vec{r},t)}{\partial t} &= \frac{D_{lip}}{k_B T} \nabla^2_{LB}(\mu_l) \end{aligned} \quad (10)$$

Here D_{lip} is the lipid diffusion coefficient that should not affect the equilibrium state, and the subscript LB denotes the Laplace-Beltrami operator (the analog of the Laplace operator on curved surfaces). The evolution of neutral lipids follows from the above equations taken together with the incompressibility relations. We stress that, in general, the CH equations are

implemented to describe time evolution of globally conserved fields. Here we do not intend to study dynamic aspects of lipid diffusion, but rather use Eqs. 10 and 9 for the sole purpose of minimizing the free energy functional F with respect to local lipid fractions. This is achieved by iteratively solving the resulting dimensionless CH equations for lipid compositions on the two leaflets:

$$\begin{aligned}\phi(\vec{r},t'+\Delta t') &= \phi(\vec{r},t') + \Delta t' \nabla'^2_{LB}\left[\ln\frac{\phi(\vec{r},t')(1-\phi^0)}{\phi^0(1-\phi(\vec{r},t'))} + z\Psi(\vec{r},t')\right] \\ &+ \Delta t' a' \kappa' (c_n^{0'} - c_c^{0'}) \nabla'^2_{LB}\left[c'(\vec{r},t') - c^{0'}(\phi(\vec{r},t'))\right]\end{aligned} \tag{11}$$

where we have used primed variables to denote the following unitless quantities:

$$t' = tD_{lip}/\xi^2; \qquad \kappa' = \kappa/k_BT; \qquad c' = c\xi; \qquad a' = a\xi^2 \tag{12}$$

where ξ is the lattice constant.

We also note that according to Eqs. 9 - 11, lipids may locally demix not only due to electrostatic interactions with the protein but also due to their tendency to preferentially form different spontaneous shapes. As an example, monovalent acidic PS, or poly-valent PIP_2 lipids have inherent positive spontaneous curvature at neutral pH(11), and therefore are expected to associate into positively curved membrane regions. Neutral PC lipids, on the other hand, would prefer negatively curved membrane patches(11). Therefore, it is obvious that an additional minimization of the free energy functional with respect to membrane shape is necessary and that the procedure should be carried out self-consistently together with the electrostatic and repulsive interactions, as well as with lipid mixing. This presents a formidable challenge, since in principle one has to consider all possible changes in membrane geometry, and couple these shape deformations to other degrees of

freedom.

Here, the combined scheme is used to efficiently account for bilayer deformations and self-consistently with the PB equation; together with the CH equations the method converges to the (local) minimum of the total free energy. Our strategy is based on representing the membrane shape as a linear superposition of Gaussian functions (used here as a basis set). With that, we sample membrane deformations by varying only the Gaussian amplitudes. This procedure significantly reduces the dimensionality of phase space that needs to be explored. The Gaussian's amplitudes are varried randomly, and trial moves are accepted if the free energy is reduced. To ensure self-consistency, at each trial move we solve the PB equation for the electrostatic potential. To couple shape changes to lipid demixing, we alternate the steps for membrane deformations with the CH moves for local lipid compositions. The outline of the algorithm can be found in the next section.

In several calculations reported in Results we make the simplifying assumption that the lipid composition within a membrane patch is constant and homogeneous. In such cases, there is no need to solve the CH equations for local lipid fractions, and our minimization scheme reduces to performing random moves for local membrane heights self-consistently with solving electrostatic problem. In addition, when we discuss homogeneous mixtures (no lipid segregation), we conveniently express elastic properties of the membrane per *bilayer* and describe membrane geometry with respect to the bilayer mid-plane(see Fig.1*B*)(34, 35). In particular, we assume that the bending modulus of the bilayer $\kappa = 2\kappa_m$(34–36), and we denote the spontaneous curvature of the bilayer mid-plane by c_0. Then the elastic free energy expression in Eq.(6) of the main text simplifies to: $F_b = \frac{1}{2}\kappa \int_{A_m} dA_m (c_m - c_0)^2$(34, 35), where c_m is the local curvature of the

mid-plane and the integration is carried out over the bilayer mid-plane surface.

To introduce the N-helix membrane interaction in our model, an additional energy term must be added to the free energy functional (Eq.(2) of the main text) in a manner similar to the work in Ref.(9, 10), and the coupling between peptide insertion and BAR interaction must be considered in the self-consistent form adopted in the model. However, the nature of the coupling among these degrees of freedom is not known, which makes the formulation of a free energy functional that can couple the electrostatic and elastic degrees of freedom that will also include peptide insertions quite challenging. Here we use a simplified approach to couple the N-helix inclusions to the electrostatic contributions, by modeling insertion effects implicitly. Thus, we define a locally positive spontaneous curvature region on the bilayer adjacent to the adsorbing BAR domain (shown in Fig. 3 of the main text), and use a phenomenological approach that assumes that the inclusions (two insertions per BAR dimer) perturb the bilayer asymmetry and its elastic properties primarily around the area of insertion(9). We account for insertions at different depths by varying the value for the spontaneous curvature assigned to this local membrane region(10). For each insertion depth, the bilayer adjusts its geometry locally, and the deformations at steady state for each penetration depth is found by minimizing the modified free energy functional which now contains an elastic free energy term that accounts for the non-zero spontaneous curvature region near the adsorbed BAR dimer.

Basic steps in the free energy minimization algorithm

In this section we detail the basic steps in the free energy minimization algorithm. Our method is based on the idea that any two-dimensional surface

shape can be represented by a linear combination of a suitable set of analytical functions, called the basis set(see for example (37, 38)). One common choice, used here, is the basis set of Gaussian functions(38). Imagine N two-dimensional Gaussians centered at different locations and each having the following functional form:

$$g_i(x,y) = A_i \times \exp\left[-\left(\frac{(x-x_i^0)^2}{\sigma_{xi}^2} + \frac{(y-y_i^0)^2}{\sigma_{yi}^2}\right)\right], \qquad i = 1, ...N. \quad (13)$$

where the *i-th* Gaussian is centered at (x_i^0, y_i^0), and its amplitude and two variances, along x and y directions, are A_i, σ_{xi} and σ_{yi} respectively. Then the height with respect to a flat reference plane of the bilayer mid-surface at point (x,y) can be approximated as a linear superposition of these Gaussian functions:

$$h(x,y) \approx \sum_{i=1}^{N} g_i(x,y) \quad (14)$$

Eq. 14 becomes exact as $N \to \infty$. The advantage here is that, with a careful choice of N and all (x_i^0, y_i^0)-s (see the next section, Simulation Details), it becomes sufficient to systematically vary only the Gaussian's amplitudes and variances in order to efficiently sample membrane deformations. This procedure significantly reduces the dimensionality of the phase space one has to explore. To further simplify calculations, we set σ_x and σ_y variances of all N Gaussians to be identical and fixed, so that we perform the sampling procedure only on the Gaussian's amplitudes.

The algorithm starts with designing a membrane mid-surface of certain initial geometry using Eqs. 13 and 14. With parallel translation, we obtain the locations of the two charged surfaces: the upper and lower leaflets(see Fig. $1B$ of the main text). We then place the desired number of lipids in both leaflets by creating suitable charge densities on the two layers; usually we start with a homogeneous distribution of lipids on both leaflets. With

the membrane geometry fixed, the BAR dimer is positioned in the desired orientation near the membrane, and Cahn-Hilliard moves are performed to vary the local lipid compositions(1), and to achieve lipid demixing under the influence of the electrostatic forces from the BAR and the elastic forces, which act to locally separate lipids according to their spontaneous curvature values. To achieve self-consistency, the non-linear PB equation is solved after each CH step to update the electrostatic potential in space. This iterative process is repeated until significant lipid segregation is observed(1), usually for 300-400 steps, depending on the lipid content.

Then, we fix the lipid composition and perform trial moves on the membrane shape by executing the following steps:

1) With the BAR fixed in the same orientation as during the CH procedure, solve the non-linear PB equation.

2) The electrostatic, bending, lipid mixing and repulsive energy contributions are calculated to obtain the adsorption free energy of the BAR-membrane complex:

$$\Delta F_{old} = F^{old}_{complex} - F_{reference} \tag{15}$$

Here $F^{old}_{complex}$ is the total free energy of the complex, and $F_{reference}$ is the total free energies of the BAR-membrane reference state.

3) Randomly pick the i-th Gaussian, and attempt to change its amplitude $A^{new}_i = A^{old}_i + \Delta r$, where Δr is a uniform random number in the range [-1;1].

4) Using the updated list of Gaussian amplitudes, construct a trial configuration of the bilayer mid-surface and upper and lower leaflets.

5) Position BAR as in step 1 next to the trial membrane and calculate the adsorption free energy of the BAR-membrane complex, ΔF_{new}. Note that the lipid composition does not change between old and trial configurations.

6) If $\Delta F_{new} \leq \Delta F_{old}$, accept the trial configuration of the membrane

and go to step 3. If $\Delta F_{new} > \Delta F_{old}$, discard the trial configuration and go to step 3.

Steps 3-6 are repeated until the membrane locally adopts its shape with respect to particular existing lipid distribution. Then, fixing the membrane geometry, we again perform Cahn-Hilliard iterations to relax the local lipid compositions, which is followed by trial steps for varying bilayer shape.

The entire loop is repeated multiple times and convergence of the algorithm to equilibrium is verified by confirming that there is no change, within numerical uncertainty, in the adsorption free energy with additional steps. Because in the algorithm the system is driven along a free energy gradient, it is tacitly assumed here that the balance of bending, electrostatic, lipid mixing and repulsive contributions exists only in one particular configuration, i.e. that the landscape of the free energy functional as defined in Eq.2 of the main text has only a single minimum. The validity of this assumption is supported by our test calculations with different initial membrane shapes. Thus, we performed the minimization procedure on BAR/membrane systems where the membrane was initially either flat or had substantial spherical deformation in the region near the adsorbed BAR. The results indicated that both starting points converged to the same final structure, however we found that the convergence from the pre-formed spherical configuration was faster. Therefore, we used membranes with pre-formed spherical domes as the initial starting point for all the simulations reported here.

We also note that any change in membrane shape will be accompanied by change in number of lipids in the simulation cell. In order to maintain a constant charge density on the two leaflets, we imagine the simulation box being coupled to a large lipid reservoir that can constantly exchange lipids with the central cell. Accordingly, at each of shape perturbation we correct the free energy functional in Eq.2 of the main text by the standard term

$\Delta f = -\Delta N \times f_{bulk}$(39), where $\Delta N = N_{new} - N_{old}$ is the difference in lipid number in the trial and current states, and f_{bulk} is the free energy per lipid in the bulk membrane (away from the adsorbed BAR).

Simulation details

We consider here the BAR domain from the Amphiphysin protein (PDB ID code 1URU) and represent it in full-atomistic 3D details, by assigning to each atom a radius and a partial charge. This BAR module contains 12 positive residues along its concave surface, and thus is characterized by a higher charge density on the membrane-facing side as compared with other BAR domains (see Fig.1 of the main text)(12).

The BAR is fixed in space near the membrane in an orientation with its long axis parallel to the flat membrane's (x,y) plane, and the short axis perpendicular to that plane (along z) as depicted in Fig. 1B. Calculations for different BAR orientations revealed that such positioning of the BAR next to membranes compared to any tilted orientation resulted in the most favorable binding free energies and largest membrane deformations (data not shown). We do not explicitly consider the amphiphatic N-terminal helices of the BAR domain, but instead, model the effects of the N-helical insertions implicitly through their effect on the membrane elastic properties.

We focus on lipid membranes of 30:70 PS/PC ($\phi = 0.3$), and 4:96 PIP_2/PC ($\phi = 0.04$) average compositions. Assuming an area per lipid headgroup of a=65Å^2 for all lipids, these mixtures correspond to charge densities of $\sigma \sim -0.004e$ and $\sigma \sim -0.0025e$ respectively. Our choices of membrane compositions are motivated by the following: 1) 30:70 PS/PC is a biologically relevant composition that mimicks the model membrane used in atomsitic simulations by Blood et al (40, 41); 2) The average composi-

tional range of PIP_2 lipids is known to be 1%-5% (8). In agreement with experimental observations (3), we have recently demonstrated(1) that, as charged proteins diffuse on a 75:24:1 PC/PS/PIP_2 membrane, they primarily sequester PIP_2 lipids, whereas the PS lipid distribution remains largely uneffected by the adsorbed protein. Thus, exploring PS- vs. PIP_2-containing mixtures enables us to specifically address the role of lipid sequestration in the process of membrane remodeling by BAR domains. To make numerical calculations simpler, we consider here both model membranes as binary mixtures of both 4:96 PIP_2/PC and 30:70 PS/PC.

The spontaneous curvatures of PS and PC lipids were set to c^0_{PS}=1/144 Å^{-1} and c^0_{PC}=-1/100 Å^{-1} respectively, values that were also reported in the literature(11, 42–44). The spontaneous curvature of PIP_2 lipid is not known from experimental measurements. We assume here $c^0_{PIP_2}$=1/70 Å^{-1}, in light of the substantial difference in head group size between PIP_2 and monovalent PS.

For all calculations the lipid membrane was modeled as a low dielectric slab ($\epsilon_m = 2$) of dimensions 256Å $\times$ 256Å $\times$ 40Å. Electrostatic calculations were performed using a modified version of the publicly available open source software: APBS version 0.4.0(45). The system was placed on a 256Å $\times$ 256Å $\times$ 256Å cubic grid with grid spacing of 1Å, and the non-linear PB was discretized with the finite-difference method. The APBS software was modified to include periodic boundary conditions in the (xy) bilayer in-plane directions. The charge, ion accessibility, and dielectric maps were configured and supplied to APBS. After each MC or CH step in the free energy minimization procedure, these maps were updated and fed back to the PB solver to obtain new electrostatic potential.

The periodic box contained 1:1 electrolyte solution of n_0 =0.1M concen-

tration, corresponding to a Debye length of $\lambda_D \approx 10$Å:

$$\lambda_D = \left(\frac{\epsilon_0 \epsilon_w k_B T}{2e^2 n_0} \right)^{1/2} \tag{16}$$

Here k_B is Boltzmann's constant, T=300K - the temperature, e - the elementary charge, ϵ_0 - the permeability of free space, and $\epsilon_w = 80$ is the dielectric constant of the aqueous solution.

As a basis set for the minimization procedure, we chose N=841 Gaussians placed equidistant from each-other on a two-dimensional (x,y) grid 9Å apart. The variances σ_x and σ_y for all Gaussians were taken as 20Å. This setup not only ensured complete coverage of the membrane surface by the Gaussians, but also provided strong overlap between neighboring Gaussian functions and made the minimization scheme efficient. Further, we used the intrinsic 2-fold symmetry of the BAR domain so that step 3 in the Monte Carlo algorithm (see previous section) was carried out simultaneously and in an identical manner on two symmetrically situated Gaussians.

The free energy minimization cycles were performed repeatedly until we observed no change, within numerical uncertainty, in the adsorption free energy with additional steps, implying no changes in lipid distribution and in membrane shape with further iterations.

References

1. Khelashvili, G., H. Weinstein, and D. Harries. 2008. Protein Diffusion on Charged Membranes: A Dynamic Mean-Field Model Describes Time Evolution and Lipid Reorganization. *Biophys. J.* 94:2580-2597.

2. Wang. J., A. Gambhir, G. Hangyas-Mihalyne, D. Murray, U. Golebiewska, and S. McLaughlin. 2002. Lateral sequestration of phosphatidylinositol 4,5-biphosphate by the basic effector domain of mystoylated alanine-rich C Kinase substrate is due to nonspecific electrostatic interactions. *J. Biol. Chem.* 277:34401-34412.

3. Golebiewska, U., A. Gambhir, G. Hangyas-Mihalyne, I. Zaitseva, J. Radler, and S. McLaughlin. 2006. Membrane-Bound basic peptides sequester multivalent (PIP_2), but not monovalent (PS), acidic lipids. *Biophys. J.* 91:588-599.

4. Haleva, E., N. Ben-Tal, and H. Diamant. 2004. Increased concentration of polyvalent phospholipids in the adsorption domain of a charged protein. *Biophys. J* 86:2165-2178.

5. Wang J. A. Gambhir, S. McLaughlin, and D. Murray. 2004. A computational model for the electorstatic sequestration of $PI(4,5)P_2$ by membrane-adsorbed based peptides. *Biophys. J.* 86:1969-1986.

6. McLaughlin, S., and D. Murrray. 2005. Plasma membrane phosphoinositide organization by protein electrostatics. *Nature* 438:605-611.

7. Tzlil, S., and A. Ben-Shaul. 2004. Increased concentration of polyvalent phospholipids in the adsorption domain of a charged protein. *Biophys. J.* 89:2165-2178.

8. McLaughlin, S., J. Wang, A. Gambhir, and D. Murray. 2002. PIP_2 and proteins: interactions, organization, and information flaw. *Annu. Rev. Biophys. Struct.* 31:151-75.

9. Zemel, A., A. Ben-Shaul, and S. May. 2005. Pertrubation of a lipid membrane by amphiphatic peptides and its role in pore formation. *Eur. Biophys. J.* 34:230-242.

10. Campelo, F., H.T. McMahon, and M. M. Kozlov. 2008. The hydrophobic insertion mechanism of membrane curvature generation by proteins. *Biophys. J.* 95:2325-2339.

11. Zimmerberg, J., and M. M. Kozlov. 2006. How proteins produce cellular membrane curvature. *Nature Reviews: Mol. Cell. Biol.* 7:9-19.

12. Peter, B. J., H. M. Kent, I. G. Mills, Y. Vallis, P. J. G. Butler, P. R. Evans, and H. T. McMahon. 2004. BAR domains as sensors of membrane curvature: the Ampiphysin BAR structure. *Science* 303:495-499.

13. Gallop, J. L., and H. T. McMahon. 2005. BAR domains and membrane curvature: bringing your curves to the BAR. *Biochm. Soc. Symp.* 72:223-231.

14. Itoh, T., and P. De Camilli. 2006. BAR, F-BAR (EFC) and ENTH/ANTH domains in the regulation of membrane-cytosol interfaces and membrane curvature. *BBA* 1761:897-912.

15. Gallop, J. L., C. C. Jao, H. M. Kent, P. J. G. Butler, P. R. Evans, R. Langen and H. T. McMahon. 2004. Mechanism of endophilin N-BAR domain-mediated membrane curvature. *EMBO* 25:2898-2910.

16. Farsad, K., N. Ringstad, K. Takei, S. R. Floyd, K. Rose, and P. De

Camilli. 2001. Generation of high curvature membranes mediated by direct endophilin bilayer interactions. *JCB* 155(2):193-200.

17. Masuda, M., S. Takeda, M. Sone, T. Ohki, H. Mori, Y. Kamioka, and N. Mochizuki. 2006. Endophilin BAR domain drives membrane curvature by two newly identified structure-based mechanisms. *EMBO* 25:2889-2897.

18. Ford, M. G. J., I. G. Mills, B. J. Peter, Y. Valls, G. J. K. Praefcke, P. R. Evans, and H. T. McMahon. 2002. Curvature of clathrin-coated pits driven by epsin. *Nature* 419:361-366.

19. Lee, M. C. S., L. Orci, S. Hamamoto, E. Futal, M. Ravazzola, and R. Schekman. 2005. Sar1p N-terminal helix initiates membrane curvature and completes the fission of a COPII vesicle. *Cell* 122:605-617.

20. Nie, Z., D. S. Hirsch, R. Luo, X. Jian, S. Stauffer, A. Cremesti, J. Andrade, J. Lebowitz, M. Marino, B. Ahvazi, J. E. Hinshaw, and P. A. Randazzo. 2006. A BAR domain in the N terminus of the Arf GAP ASAP1 affects membrane structure and trafficking of epidermal growth factor receptor. *Curr. Biol.* 16:130-139.

21. Fernandes, F., L. M. S. Loura, F. J. Chichon, J. L. Carrascosa, A. Fedorov, and M. Prieto. 2008. Role of Helix-0 of the N-BAR domain in membrane curvature generation. *Biophys. J.* 94:3065-3073.

22. Sharp, K. A., and B. Honig. 1990. Electrostatic interactions in macromolecules: theory and applications. *Annu. Rev. Biophys. Chem* 19:301-32.

23. Andelman, D. 1995. Electrostatic properties of membranes: The Poisson-Boltzmann theory. 1B 603-642. Handbook of Biological Physics. Elsevier Science B.V., Amsterdam.

24. Reiner, E.S., and C.J. Radke. 1990. Variational approach to the electrostatic free energy in charged colloidal suspensions: general theory for open systems. *J. Chem. Soc., Faraday Trans.* 86:3901-3912.

25. Honig, B., and A. Nicholls. 1995. Classical electrostatics in Biology and Chemistry. *Science.* 268:1144-1149.

26. Borukhov, I., D. Andelman, and H. Orland. 1997. Steric Effects in Electrolytes: A Modified Poisson-Boltzmann Equation. *Phys. Rev. Lett.* 79:435-438.

27. Fogolari, F., and J. M. Briggs. 1997. On the variational approach to the Poisson-Boltzmann free energies. *Chem. Phys. Lett.* 281:135-139.

28. Murray, D., A. Arbuzova, B. Honig, and S. McLaughlin. 2002. The role of electrostatic and nonpolar interactions in the association of peripheral proteins with membranes. *Current Topics in Membranes.* Volume 52. Chapter 10. pp:277-307.

29. Chaikin, P.M. and T.C. Lubensky, 2000. Principles of Condensed Matter Physics. Cambridge university press, Cambridge.

30. Chandrasekar, S. 1943. Stochastic problems in physics and astronomy. *Rev. Mod. Phys.* 15:1-89.

31. Krishna, R., and J. A. Wesselingh. 1997. The Maxwell-Stefan approach to mass transfer. *Chem. Engin. Sci.* 52:861-911.

32. Harries, D., S. May, and A. Ben-Shaul. 2003. Curvature and charge modulations in lamellar DNA-lipid complexes. *J. Phys. Chem. B.* 107:3624-3630.

33. May, S., D. Harries, and A. Ben-Shaul. 2000. Lipid demixing and protein-protein interactions in the adsorption of charged proteins on mixed membrane. *Biophys. J.* 79:1747-1760.

34. Siegel, D. P., and M. M. Kozlov. 2004. The Gaussian Curvature Elastic Modulus of N-Monomethylated Dioleoylphosphatidylethanolamine: Relevance to Membrane Fusion and Lipid Phase Behavior *Biophys. J.* 87:366 - 374.

35. Marsh, D. 2006. Elastic curvature constants of lipid monolayers and bilayers. *Chem. Phys. Lip.* 144:146-159.

36. Petrache, H. I., D. Harries, and V. A. Parsegian. 2005. Alteraion of lipid membrane rigidity by cholesterol and its metabolic precursors. *Macromol. Symp.* 219:39-50.

37. Davidson, E. 1986. Basis set selection for molecular calculations. *Chem. Rev.* 86(4):681-696.

38. Leach, A. 1996. Molecular modelling: principle and applications. Singapore: Longman.

39. Harries, D., and V. A. Parsegian. 2004. Gibbs adosption isotherm combined with Monte Carlo sampling to see the action of cosolutes on protein folding. *Proteins* 57:311-321.

40. Blood, P. D., and G. A. Voth. 2006. Direct observation of Bin/amphiphysin/Rvs (BAR) domain-induced membrane curvature by means of molecular dynamics simulations. *PNAS* 103(41):15068-15072.

41. Blood, P. D., R. D. Swenson, and G. A. Voth. 2008. Factors infuencing local membrane curvature induction by N-BAR domains as revealed by molecular dynamics simulations. *Biophys. J.* 95:1866-1876.

42. Fuller, N., Benatti, C.R., and Rand, R.P. 2003. Curvature and bending constants for phosphatidelserine-containing membranes. *Biophys. J.* 85:1667-1674.

43. Chen, Z., and Rand, R.P. 1997. The influence of cholesterol on phospholipid membrane curvature and bending elasticity. *Biophys. J.* 73:267-276.

44. Szule, J. A, Fuller, N.L., and Rand, R.P. 2002. The effects of acyl chain length and saturation of diacylglycerols and phophatidylcholines on membrane monolayer.*Biophys. J.* 83:977-984.

45. Baker, N. A., D. Sept, S. Joseph, M. J. Holst, and J. A. McCammon. 2001. Electrostatics of nanosystems: application to microtubules and the ribosome. *Proc. Natl. Acad. Sci. USA* 98:10037-10041.

Figure Captions

Figure S1. Adsorption of the Amphiphysin BAR domain on membranes of $\sigma = -0.004e/\text{Å}^2$ average surface charge density ($\phi^0_{PS} = 0.3$) and with preformed spherical deformation. The variation in the binding free energy (in k_BT units) is shown versus the radius of the spherical cap. Inset depicts the BAR (in ball-and-stick representation) adsorbed onto a membrane deformed into a spherical cap of R=100 Å (green). We show only the portion of the membrane's upper leaflet neighboring the BAR, close to the spherical deformation. The membrane shape smoothly transitions to the flat state in the bulk.

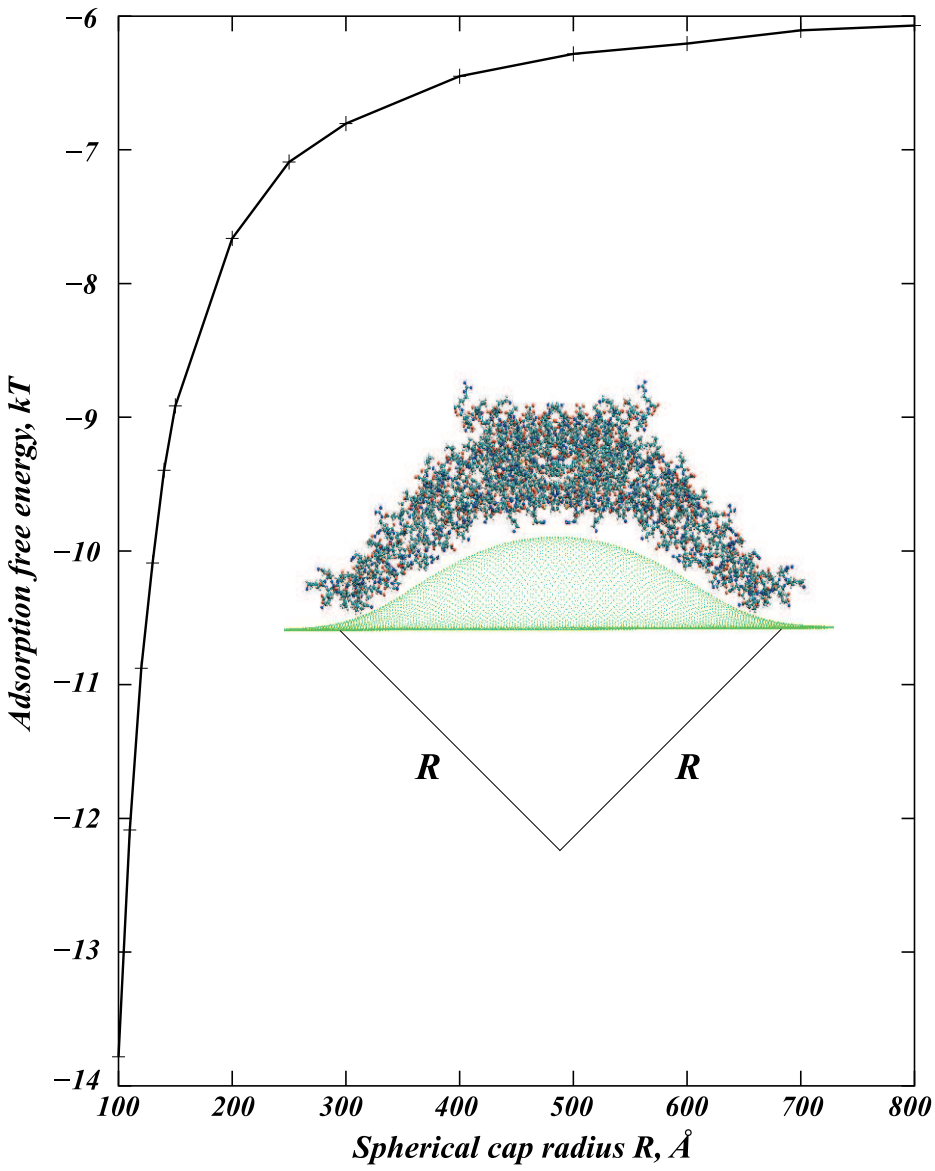

Figure S1 **(GK, HW and DH)**